AD-A150 886 MULTIPLE PRODUCT CHANNELS IN THE COLLISION FREE UV PHOTODISSOCIATION OF 2-NITROPROPANE(U) UNIVERSITY OF SOUTHERN CALIFORNIA LOS ANGELES DEPT OF CHEMIST.. 1/1

UNCLASSIFIED C WITTIG 01 APR 84 N00014-80-C-0539 F/G 7/5 NL

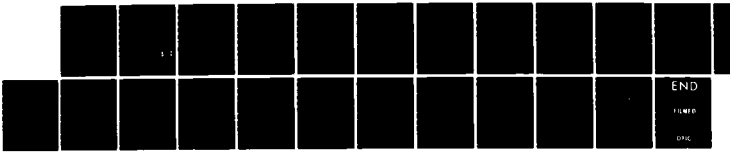

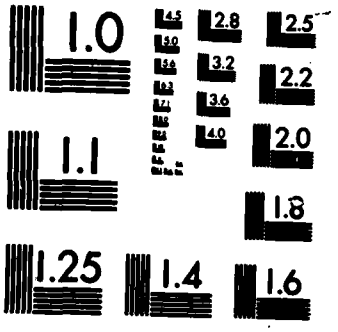

MICROCOPY RESOLUTION TEST CHART
NATIONAL BUREAU OF STANDARDS-1963-A

Unclassified

(2)

SECURITY CLASSIFICATION OF THIS PAGE (When Data Entered)

REPORT DOCUMENTATION PAGE		READ INSTRUCTIONS BEFORE COMPLETING FORM
1. REPORT NUMBER	2. GOVT ACCESSION NO.	3. RECIPIENT'S CATALOG NUMBER
4. TITLE (and Subtitle) MULTIPLE PRODUCT CHANNELS IN THE COLLISION FREE UV_PHOTODISSOCIATION OF 2-NITROPROPANE		5. TYPE OF REPORT & PERIOD COVERED Annual Report 4/1/83-3/31/84
		6. PERFORMING ORG. REPORT NUMBER
7. AUTHOR(s) Curt Wittig		8. CONTRACT OR GRANT NUMBER(s) N00014-80-C-0539
9. PERFORMING ORGANIZATION NAME AND ADDRESS University of Southern California Los Angeles, CA 90089		10. PROGRAM ELEMENT, PROJECT, TASK AREA & WORK UNIT NUMBERS
11. CONTROLLING OFFICE NAME AND ADDRESS Dr. Richard Miller, Office of Naval Res. Code 432, 800 N. Quincy Street Arlington, VA 22217		12. REPORT DATE 4/1/84
		13. NUMBER OF PAGES 23
14. MONITORING AGENCY NAME & ADDRESS(if different from Controlling Office)		15. SECURITY CLASS. (of this report) Unclassified
		15a. DECLASSIFICATION/DOWNGRADING SCHEDULE

16. DISTRIBUTION STATEMENT (of this Report)

Unlimited

DISTRIBUTION STATEMENT A
Approved for public release;
Distribution Unlimited

17. DISTRIBUTION STATEMENT (of the abstract entered in Block 20, if different from Report)

18. SUPPLEMENTARY NOTES

Cont'd

DTIC ELECTE FEB 27 1985 S D

19. KEY WORDS (Continue on reverse side if necessary and identify by block number)

nitropropane, collision free, photodissociation, nitroalkanes, photolysis, linear.

20. ABSTRACT (Continue on reverse side if necessary and identify by block number)

The 1-photon, collision-free, UV (222, 249, and 308 nm) photodissociation of 2-nitropropane leads to several chemically distinct sets of products. We report the detection of OH, HONO, and NO_2, and discuss mechanisms, as well as implications concerning condensed phase reactions.

DD FORM 1 JAN 73 1473 EDITION OF 1 NOV 65 IS OBSOLETE

unclassified

SECURITY CLASSIFICATION OF THIS PAGE (When Data Entered)

85 02 12 097

AD-A150 886

DTIC FILE COPY

N00014-80 C-0539

MULTIPLE PRODUCT CHANNELS IN THE COLLISION FREE UV PHOTODISSOCIATION OF 2-NITROPROPANE

Curt Wittig

Chemistry Department
University of Southern California

I. INTRODUCTION

Establishing the pathways and mechanisms for the decomposition of 'nitro' compounds in the gaseous and/or condensed phases is an arduous, yet entirely worthwhile endeavor. Initially, interest centered around determining the C-N bond strength of nitroalkanes,[1-3] and more recently around the physical and chemical processes which are germane to the exothermic decompositions of energetic materials.[4-18] However, such dissociation processes are of fundamental importance, since several distinct pathways are energetically accessible, and the chemical processes which accompany the spreading of an initially localized excitation are important in many contexts.

Several studies involving thermally driven reactions of nitroalkanes indicate that rupture of the C-N bond as the primary dissociation step is exclusive to nitromethane, with the decomposition of other mononitroalkanes resulting in the production of the corresponding alkene. Most of these studies were carried out at pressures of several Torr, and temperatures of 700-1000K. It was suggested that alkene production occurred by the elimination of nitrous acid (HONO) via a 5-membered ring transition state,[5-11] and the formation of other pyrolysis products such as NO and NO_2 is consistent with such a mechanism, if it is assumed that HONO initiates a chain of secondary reactions. This is sensible, considering the low bond strength (48 kcal mol^{-1}) of this species. The first study of such reactions under collision-free conditions was by Benson et

al.[19] using the very low pressure pyrolysis technique. They showed that the decomposition mechanisms for both 1- and 2-nitropropane involved propylene production. Detection of HONO was attempted, but was not entirely conclusive; a small peak at mass 47 was observed, and from this it was inferred that very little of the HONO survived the high temperature of the reactor.

In the experiments reported herein, we present our initial results concerning the different photodissociation pathways which accompany the UV photolysis (222, 249, and 308 nm) of 2-nitropropane (2NP), under collision-free conditions. Since there are no nitrogen atom lone pair electrons, excitation involves the promotion of an oxygen atom lone pair electron into an antibonding π^*-group orbital. Even though the subsequent radiationless transition out of S_1 is rapid, the nuclear motions which commence upon absorption of a photon cause the nuclei to reconfigure, particularly in the vicinity of the NO_2 group. The radical-like nature of the oxygen can facilitate the formation of a 5-membered ring, which can lead to products such as OH and HONO, and NO_2 can also be liberated efficiently before the nuclear energies dissipate into the vibrational reservoir of the propyl radical. We find that all three of these products are produced at each of the photolysis wavelengths, and that OH is a nascent product in all instances. This capacity of the system to produce a well known chain carrier such as OH may be a key to understanding the initial stages of the decomposition of energetic materials in condensed phases.

Originator Supplied Keywords Include:
(See DD1473 (Field 19))

II. EXPERIMENTAL METHODS

By now, the experimental arrangement used in the type of work reported below has become familiar,[20] and only a brief description will be given here. Gaseous samples are passed through a chamber designed for LIF detection, and photodissociation is effected with the unfocused UV output from an excimer laser (Lumonics 860; 222, 249, and 308 nm). The absorption coefficient for room temperature 2NP (Fig. 1(a)) is modest at 249 and 308 nm and rather large at 222 nm, and the available laser fluences are adequate for dissociating a reasonable fraction of the material in the beam (~0.05% with 25 mJ cm^{-2} at 249 nm). The sample is probed at right angles to the photolysis beam with beams derived from a Nd:YAG laser system. A 355 nm beam (typically several mJ) counterpropagates with, and precedes by 6 ns, the tunable radiation from a doubled dye laser (308-310 nm), which is used to detect $OH(X^2\Pi)$ via LIF on the (0,0) band of the $A^2\Sigma^+ \leftarrow X^2\Pi$ system. None of the laser beams are focused in the work reported here. The delay between the excimer and Nd:YAG lasers is controlled digitally (jitter = ±20 ns) and the shortest delay used was 40 ns. Signals are processed using a boxcar integrator (PAR 162/165).

HONO samples are used for calibration purposes and are prepared by dropping aqueous H_2SO_4 solution (10% M) into aqueous sodium nitrite (0.01 M), in a flow system.[21] Products enter the main vacuum chamber through a capillary (10 cm x 0.08 mm^2) which serves to restrict the flowrate and stabilize the HONO

concentration. HONO prepared in this way is not pure, but in equilibrium with H_2O, NO_2, NO, etc. However, we find that this method of preparing HONO is more convenient than using an equilibrium mixture made from H_2O, NO_2, and NO.[22,23] GCMS analyses of 2-nitropropane (Merck, 96%) indicate that 1-nitropropane is the only impurity.

III. RESULTS

A. Nascent OH ($X^2\Pi$)

The photolysis of 2NP was carried out at three convenient excimer laser wavelengths (222, 249, and 308 nm), and the detection of OH($X^2\Pi$) was via LIF on the (0,0) band of the $A^2\Sigma^+ \leftarrow X^2\Pi$ system. With 249 and 308 nm photolysis, the S/N was sufficient to determine the dependences of the peak LIF signals on pressure and/or delay. These measurements indicate clearly that OH is produced by a collision-free process. With a 40 ns delay between the photolysis and probe lasers, the peak OH LIF signal intensity (monitoring the $Q_1(2)$ line) varied linearly with the 2NP pressure over the range 30-300 mTorr. Also, with the 2NP pressure fixed at 200 mTorr, no change in OH LIF signal intensity was observed for delays of 40-1000 ns. With delays >1 μs, the variation of the peak OH LIF signal intensity with delay is different for the 249 nm and 308 nm photolysis wavelengths. With 249 nm photolysis, the OH LIF signal increases by 40% up to delays of 20μs, after which the signals decrease due to the diffusion of molecules out of the detection region. Rotational relaxation was

suspected of causing this signal increase, and this was verified by measuring the peak OH LIF signal intensity vs. delay in the presence of varying amounts of an inert buffer, which causes thermalization of the nascent rotational and translational excitations. Data which show the effects of 1,4, and 20 Torr of added He are shown in Fig. 2. The results are quite sensible, and with 20 Torr of He the signal intensity remained constant over the entire delay range. With 308 nm photolysis, there is less energy available for product R,T excitations, and the OH LIF signal does not vary significantly with delay except at long times, where diffusion removes species from the detection region. In all of these experiments, the linewidth of the probe laser is large enough (~0.7 cm^{-1}) so that all molecules within the nascent OH Doppler profile are treated equally by the probe. This insures that velocity changes do not produce a concomitant signal change.

It was possible to estimate nascent $OH(X^2\Pi)$ V,R distributions following 249 and 308 nm photolysis, and the results of one such measurement are shown in Fig 3. With 249 and 308 nm photolysis, nascent $OH(X^2\Pi, v''=0)$ could be ascribed rotational temperatures of ~370 and 230K respectively. By analyzing the region of the (1,1) band, it is possible to detect vibrational excitation, and this was done whenever the S/N permitted such observations. In all instances, $[OH(X^2\Pi, v''=1)] << [OH(X^2\Pi, v''=0)]$, and excited $OH(X^2\Pi)$ vibrational levels were not examined further. These rotational distributions are consistent with the effects discussed above and shown in Fig. 2, since the

population of N"=2 increases by 40% in going from 370 to 300K, while the same population shows no noticeable change in going from 230K to 300K. Since product internal excitations are correlated with product translational recoil in the center of mass of the parent, product internal state distributions may possess some memory for the anisotropic nature of the excitation process, and such detailed considerations will be dealt with in future experiments. For both 249 and 308 nm photolysis, the variation of the OH LIF signal with the photolysis laser fluence was quite linear over a wide range of fluences, as shown in Fig. 4. At the lowest photolysis fluences, it is not possible to saturate any dissociative transition of the parent or any conceivable photoproduct. Thus, $OH(X^2\Pi)$ derives from a 1-photon process.

Even though the 2NP absorption cross section at 222 nm is two orders of magnitude larger than that at 249 nm, the S/N following 222 nm photolysis was much lower than that at 249 nm. Thus, it was not possible to measure pressure or delay dependences, or nascent distributions, as carefully as with 249 and 308 nm photolyses. 222 nm photolysis is accompanied by an emission (either parent LIF or product chemiluminescence) which cannot be removed experimentally, and which acts as a background, thereby limiting S/N. Also, the amount of $OH(X^2\Pi)$ produced, per photon absorbed, is ~5 times less than with 249 nm photolysis, and this is discussed below. As with the other cases, the OH LIF

signals vary linearly with the photolysis laser fluence, indicating that a 1-photon process is responsible for the observations.

B. Nascent HONO

Having shown unambiguously that $OH(X^2\Pi)$ derives from the 1-photon, collision-free UV photolysis of 2NP, it remains to delineate the mechanisms whereby it is produced. Possible pathways are listed below:

$$2NP + h\nu \rightarrow 2NP^* \rightarrow C_3H_6NO + OH \quad (1)$$

$$\rightarrow C_3H_6(\text{propene}) + NO + OH \quad (2)$$

$$\rightarrow C_3H_6(\text{propene}) + HONO \quad (3)$$

as well as

$$HONO^{\ddagger} \rightarrow OH + NO \qquad \Delta H = 48 \text{ kcal mol}^{-1} \quad (4)$$

where ‡ denotes nascent vibrational excitation. The enthalpy changes for reactions (1)-(3) depend on the photolysis wavelength, and are summarized in Table I. Reaction (4) only contributes to the production of nascent $OH(X^2\Pi)$ when the nascent HONO produced via reaction (3) contains internal energy in excess of 48 kcal mol^{-1}. It is safe to assume that, under the present experimental conditions, HONO containing >48 kcal mol^{-1} of internal energy dissociates before it is collisionally deactivated. The concerted, potentially non-statistical behavior of reactions (1)-(3), as well as the propensity for dissociations which result in closed-shell products producing nascent products which are quite internally excited, makes it impossible to predict a priori the roles of reactions (3) and (4) in producing OH.

To determine if HONO is indeed a nascent product, 355 nm radiation was used to photodissociate HONO via the well-known $A^1A'' \leftarrow X^1A'$ system:[23,24]

$$HONO + h\nu \rightarrow HONO^* \rightarrow OH + NO \qquad (5)$$

We use 355 nm fluences which are sufficiently low that they do not produce measurable effects in the absence of the excimer laser radiation. Thus, by detecting OH which is produced by 355 nm photodissociation, we can monitor the presence of HONO.[20] Since nascent HONO internal excitation will affect the 355 nm absorption cross section, it is not possible to quantitatively determine HONO concentrations in these cases. However, with thermalized samples, quantitative mesurements are possible, since known concentrations of HONO can be used to calibrate the detection apparatus.[20,21]

With either 222 or 249 nm photolysis and under collision-free conditions, the presence of 355 nm radiation (20 mJ cm^{-2}) increased the OH LIF signals by ~5%. With this fluence, and assuming a 300K absorption cross section (Table I), approximately 2% of the HONO will be photodissociated. Thus, it appears that the nascent HONO concentration exceeds that of nascent OH for these photolysis wavelengths. With 308 nm photolysis, the presence of 355 nm radiation increased the OH LIF signals by approximately 30%. Here, it appears that the nascent HONO concentration exceeds the nascent OH concentration by at least an order of magnitude. In all of these experiments, there was no obvious dependence on the delay between the photolysis and

analysis lasers (40 ns, 1 μs, and 30 μs), and/or the addition of buffer gas. This indicates that the absorption cross section of nascent HONO is not affected markedly by internal excitation, which is sensible, since 355 nm lies in the central portion of the $A^1A'' \leftarrow X^1A'$ absorption system (see Fig. 1(b)).

C. Nascent NO_2

Perhaps the most conceptually straightforward of the dissociation pathways is C-N bond rupture:

$$2NP + h\nu \rightarrow 2NP^* \rightarrow C_3H_7(\text{isopropyl}) + NO_2 \qquad (6)$$

which has been shown to be an important process in the UV photodissociation of nitroalkanes.[15-18] In our experiments, NO_2 was monitored via LIF of the $\tilde{A}^2B_2 \leftarrow \tilde{X}^2A_1$ system in the region 571-572 nm, and was observed following photolysis at the three excimer laser wavelengths. Room temperature NO_2 has structured, unmistakable features in this region, making identification straightforward. However, nascent V,R excitations will blur this fingerprint, and we found that delays $\geq$30 μs were necessary in order to obtain clean, reproducible NO_2 LIF spectra. As with OH, we insured that NO_2 derived from a 1-photon, collision-free process, even though collisions were subsequently used in order to thermalize nascent V,R excitations. The long delays were also helpful in discriminating against an emission in the region of NO_2 fluorescence, which accompanies photolysis at 222 and 249 nm, but not 308 nm.

IV. DISCUSSION

From the results presented above, it is clear that a 5-membered ring is involved in at least one of the reaction pathways at each photolysis wavelength. The $OH(X^2\Pi)$ nascent product can derive from a sequential process, in which nascent HONO formed with internal energy in excess of 48 kcal mol^{-1} subsequently decomposes into OH + NO, as well as the direct attack of the reactive, radical-like oxygen atom which is prepared by photon absorption. The latter is facilitated by the proximity of the H and O atoms, and the large, localized excitation implanted initially in the NO_2 group.

The molecular elimination of HONO is the most exoergic of the different pathways, and is known to dominate for unimolecular reactions which transpire on S_0 at modest excitations.[19] Such molecular eliminations are known to leave products internally excited, and if these products contain sufficient excitation, they can dissociate without assistance from collisions. At higher excitations, other pathways become competitive, and because of the large A-factors for simple bond fission reactions, such as reaction (6), such pathways may dominate at sufficiently high excitation.

In the present experiments, the respective roles of different electronic potential surfaces is not clear. Following the absorption of a UV photon, S_1 decays non-radiatively, and although S_0 is often invoked, the states which participate in the dissociation process are undetermined for the most part. The

highly localized initial excitation in the NO_2 group, well above dissociation threshold, encourages non-statistical behavior on any potential surface which is coupled to dissociation continua. As the photolysis wavelength is decreased, the quantum yields for the channels producing HONO and NO_2 vary, and we note that the ratio [HONO]/[NO_2] increases by a factor of ~2 in going from 222 to 308 nm.

Finally, we wish to point out that the present experimental results are quite relevant to the condensed phase reactions of such materials.[4,26] Even with an isolated gaseous molecule such as 2NP, OH is readily produced and can be attributed to a 5-membered ring which yields OH either directly or by the subsequent decomposition of HONO following molecular elimination. The radical-like character of the oxygen atom which promotes formation of the 5-membered ring can play a very important role in condensed media, where species are in intimate contact. Here, there is an abundance of possible reaction pathways, and the production of OH and/or HONO is not sterically hindered as with isolated gaseous species. Thus, we expect the OH/HONO channels to open significantly relative to the NO_2 channel. Since HONO dissociation is facile, it may well be that large concentrations of OH are produced in the very early stages of decomposition, and lead to the efficient subsequent consumption of fuel, in the rapid, exothermic decomposition of an energetic material.

REFERENCES

1. H. Taylor and V. Vesselovsky, J. Phys. Chem. 39 (1935) 1095.
2. E.W.R. Steacie and W.M.F. Smith, J. Chem. Phys. 6 (1938) 145.
3. R. Cass, S.E. Fletcher, C.T. Mortimer, P.G. Quincey, and H.D. Springall, J. Chem. Soc. (1958) 958.
4. M.A. Schroeder, Proc. 16th JANNAF Comb. Meeting, CPIA Pub. No. 308, Vol. II, (1979) 17; Proc. 17th JANNAF Comb. Meeting, CPIA Pub. No. 329, Vol. II, (1980) 493; Proc. 18th JANNAF Comb. Meeting, CPIA Pub. No. 347, Vol. II, (1981) 395; Proc. 19th JANNAF Comb. Meeting, CPIA Pub. No. 366, Vol. I, (1982) 321.
5. (a) T.L. Cottrell and T.J. Reid, J. Chem. Phys. 18 (1950) 1306.
   (b) T.L. Cottrell, T.E. Graham, and T.J. Reid, Trans. Faraday Soc. 47 (1951) 584.
6. T.L. Cottrell, T.E. Graham, and T.J. Reid, Trans. Faraday Soc. 47 (1951) 1089.
7. P. Gray, Trans. Faraday Soc. 51 (1955) 1367.
8. P. Gray, A.D. Yoffe, and L. Roselaar, Trans. Faraday Soc. 51 (1955) 1489.
9. K.A. Wilde, Ind. Eng. Chem. 48 (1956) 769.
10. K.A. Wilde, J. Phys. Chem. 61 (1957) 385.
11. T.E. Smith and J.G. Calvert, J. Phys. Chem. 63 (1959) 1305
12. G.M. Nazin, G.B. Manelis, and F.I. Dubovitskii, Russian Chem. Rev. 37 (1968) 603.

13. V.I. Faustov, S.A. Shevelev, N.A. Anikin, and S.S. Yufit, Izv. Akad. Nauk. SSSR ser. Khim. 12 (1979) 2800.
14. K.G. Spears and S.P. Brugge, Chem. Phys. Lett. 54 (1978) 373.
15. P.E. Schoen, M.J. Marrone, J.M. Schnur, and L.S. Goldberg, Chem. Phys. Lett. 90 (1982) 272.
16. L.J. Butler, D. Krajnovich, Y.T. Lee, G. Ondrey, and R. Bersohn, J. Chem. Phys. 79 (1983) 1708.
17. N.C. Blais, J. Chem. Phys. 79 (1983) 1723.
18. B.H. Rockney and E.R. Grant, J. Chem. Phys. 79 (1983) 708.
19. G.N. Spokes and S.W. Benson, J. Am. Chem. Soc. 89 (1967) 6030.
20. H. Reisler, G. Radhakrishnan, D. Sumida, J. Chou, J. Pfab, I. Nadler, and C. Wittig, Israel J. Chem. (1984), in press.
21. R.A. Cox and R.G. Derwent, J. Photochem. 6 (1977) 23.
22. R. Varma and R.F. Curl, J. Phys. Chem. 80 (1976) 402.
23. R. Vasudev, R.N. Zare, and R.N. Dixon, Chem. Phys. Lett. 96 (1983) 399.
24. G.W. King and D. Moule, Can. J. Chem. 40 (1962) 2057.
25. Adapted from the Sadtler index (p. 1).
26. T.B. Brill and C.O. Reese, J. Phys. Chem. 84 (1980) 1376.

TABLE I. Absorption cross sections and reaction exothermicities relevant to the photodissociation of 2NP and HONO.

Photolysis wavelength (nm)	Photon energy (kcal mol^{-1})	Absorption cross section[a] (units of $10^{-18} cm^2$)		Excess energies (kcal mol^{-1}) for the following reactions			
		2NP	HONO	(1)	(2)	(3)	(6)
222	129	42	1.77	36	60	108	72
249	115	3.82	0.18	22	46	94	58
308	93	2.90	small	0	24	72	36
355	80	small	0.29	-13	11	59	23

[a] For 300K samples.

FIGURE CAPTIONS

1. (a) Ultraviolet spectra of liquid 2NP[25] and gaseous HONO.[21] The absorption features in 2NP are assigned to an $\pi^* \leftarrow n$ transition around 250 nm and to a $\pi^* \leftarrow \pi$ transition at shorter wavelengths.

   (b) In HONO, the structured absorption in the region 300-400 nm has been assigned to the $\tilde{A}^1A'' \leftarrow \tilde{X}^1A'$ system, and is an $\pi^* \leftarrow n$ type transition.[24]

2. LIF spectrum of OH, generated by the 249 nm photolysis of 2NP, showing rotational lines of the (0,0) Q_1-branch of the $A^2\Sigma^+ \leftarrow X^2\Pi$ system. The inset shows the rotational populations, which can be ascribed a rotational temperature of 370K.

3. Variation of the $Q_1(2)$ peak LIF signal intensity as a function of the delay between the photolysis and probe lasers. The increase of the signal intensity is attributed to rotational relaxation. This is demonstrated in (a)-(d) for the case of 249 nm photolysis, where thermalization is induced by adding varying amounts of buffer gas. The dependence observed using 308 nm photolysis is shown in (e). At this photolysis wavelength, no increase in the LIF signal intensity is observed at delays which allow collisions. This is consistent with the cooler nascent rotational distribution (see text).

4. Variation of the OH LIF signal with the photolysis laser fluence. With both 249 and 308 nm photolysis, the signals vary linearly, indicating that in both instances OH is produced by a 1-photon process.

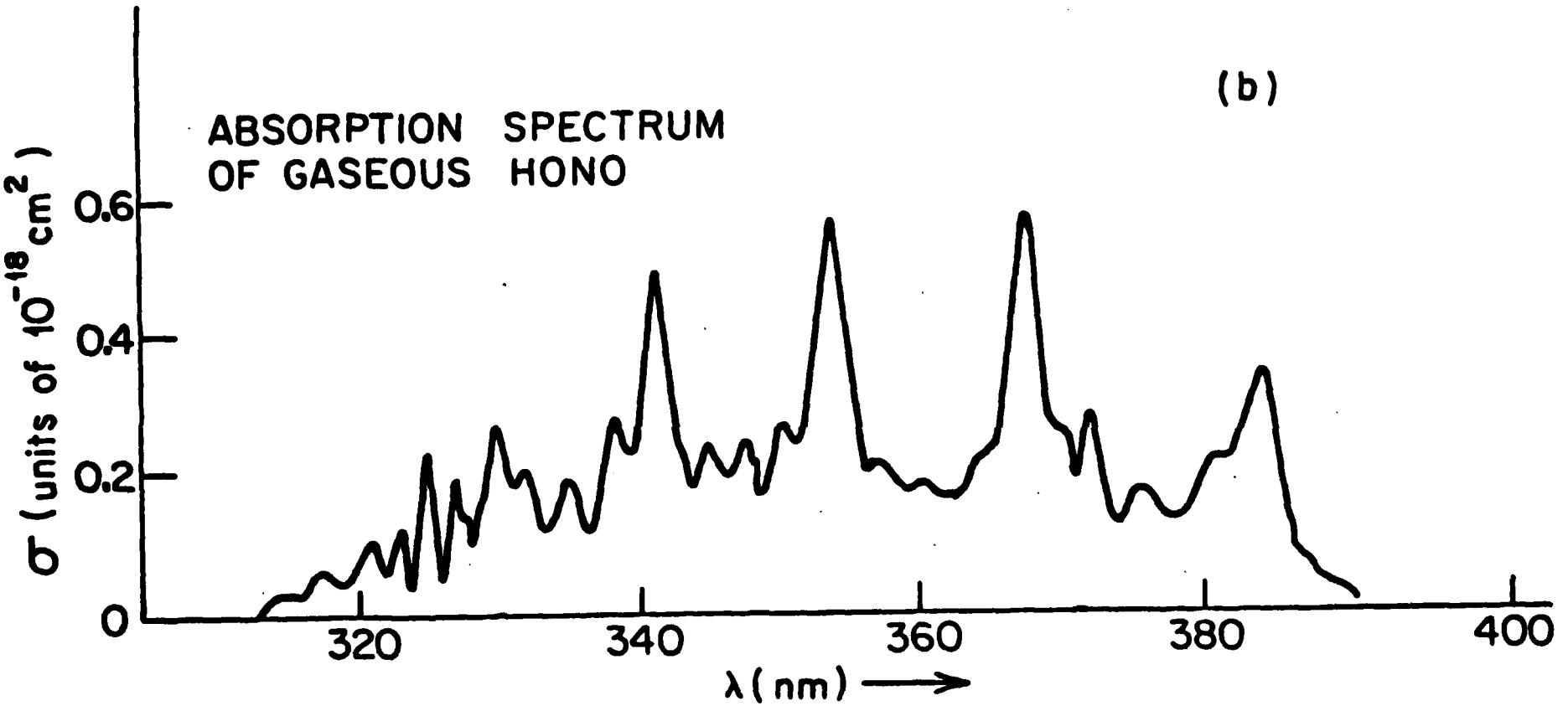
(b)
ABSORPTION SPECTRUM
OF GASEOUS HONO
σ (units of 10^{-18} cm^2)
0.6
0.4
0.2
0
320
340
360
380
400
λ (nm) ⟶

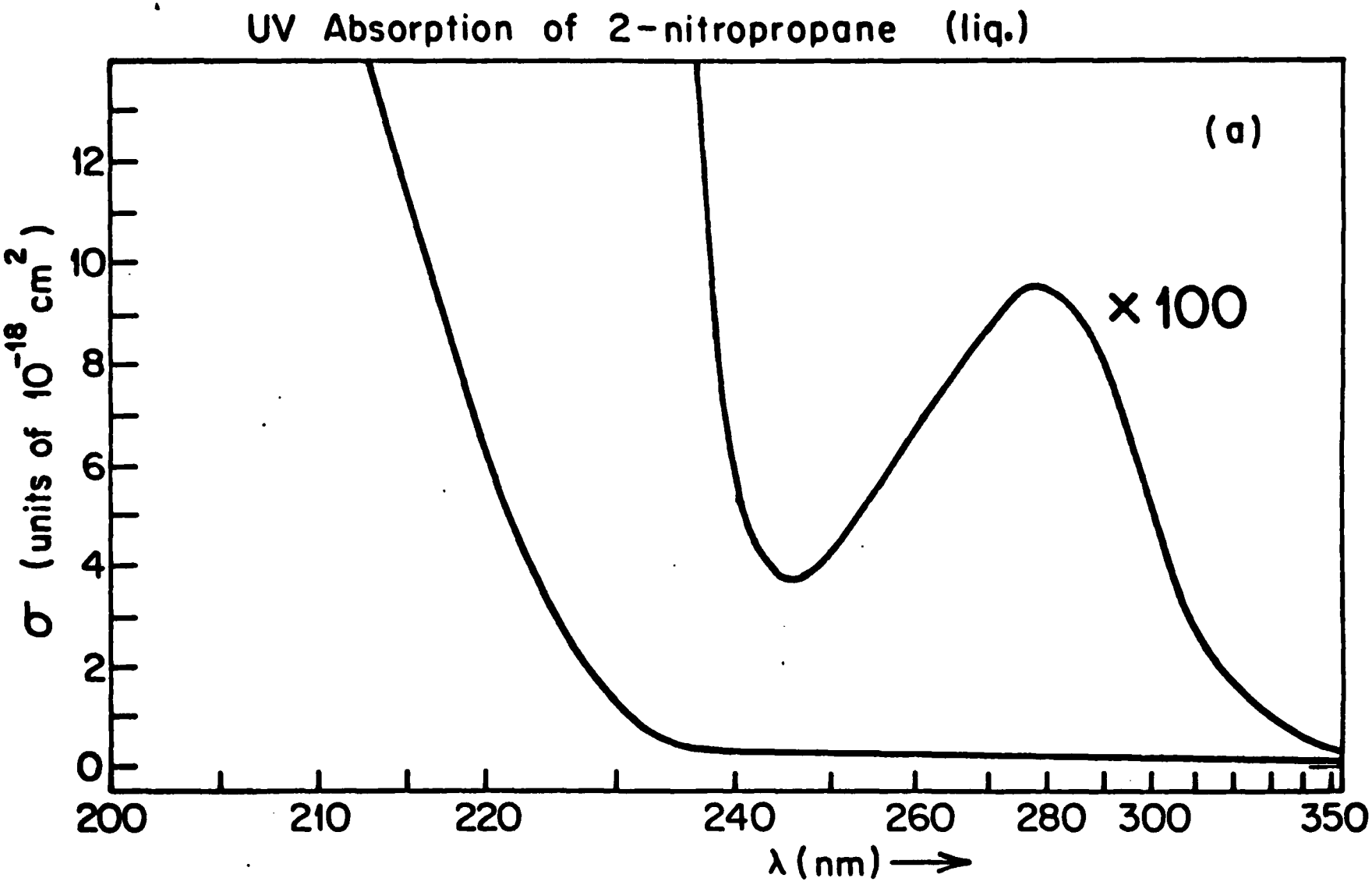
UV Absorption of 2-nitropropane (liq.)
(a)
× 100
σ (units of 10^{-18} cm^2)
0
2
4
6
8
10
12
200
210
220
240
260
280
300
350
λ (nm) ⟶

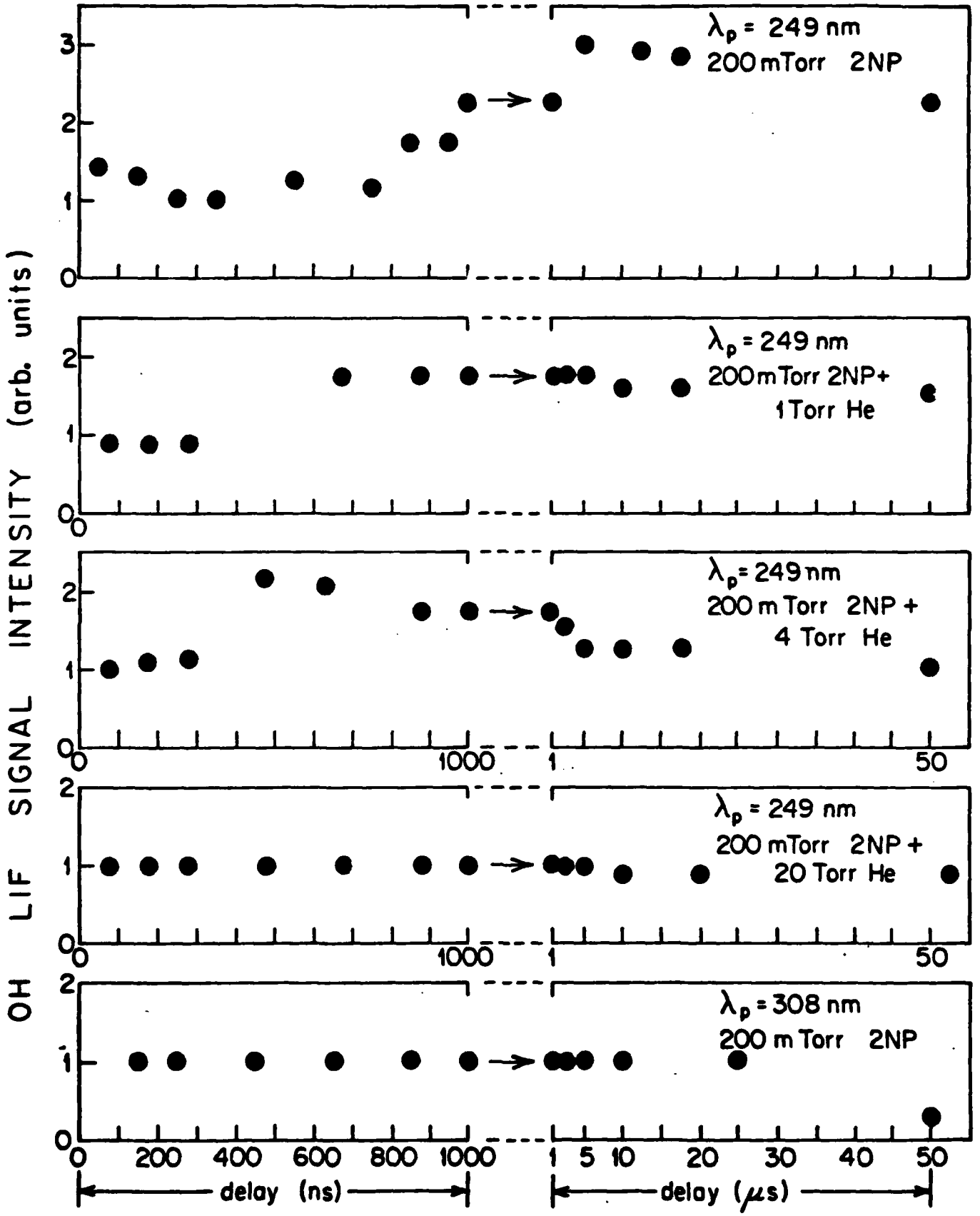
λ_p = 249 nm
200 mTorr 2NP
λ_p = 249 nm
200 mTorr 2NP+
1 Torr He
λ_p = 249 nm
200 m Torr 2NP +
4 Torr He
λ_p = 249 nm
200 mTorr 2NP +
20 Torr He
λ_p = 308 nm
200 m Torr 2NP
OH LIF SIGNAL INTENSITY (arb. units)
0 200 400 600 800 1000
1 5 10 20 30 40 50
delay (ns)
delay (μs)

OH Rotational Populations
from LIF of the
$A^2\Sigma \leftarrow X^2\Pi$, Q_1 Branch,
(0, 0) Band
200 mTorr 2-Nitropropane
40 ns delay

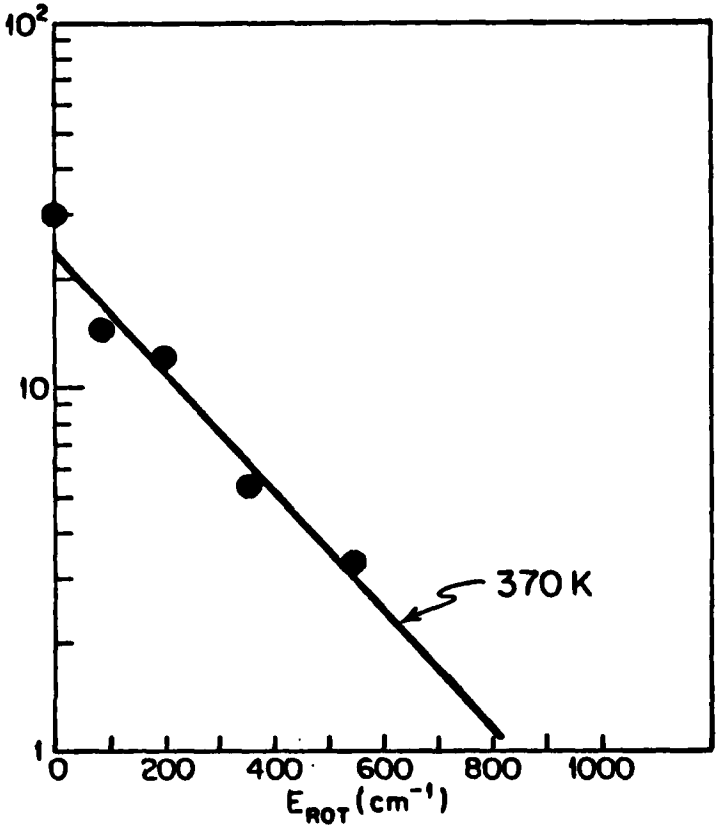

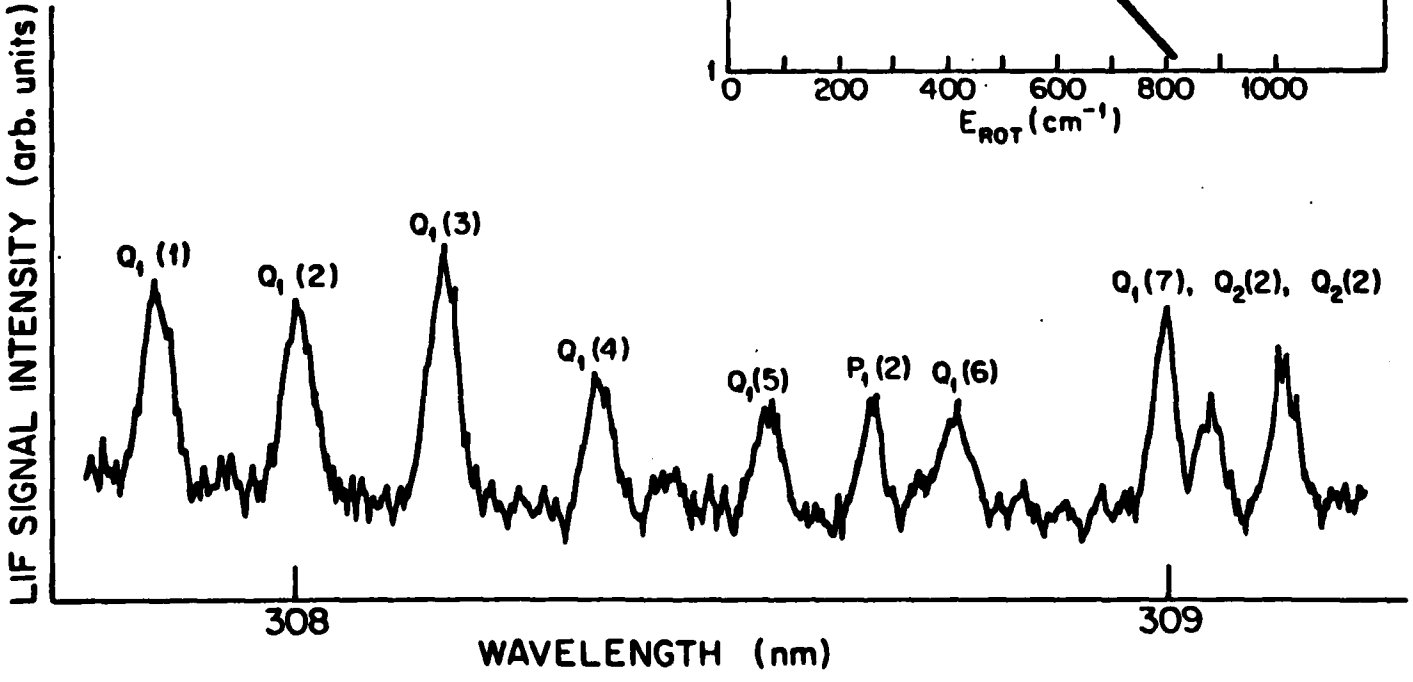

32

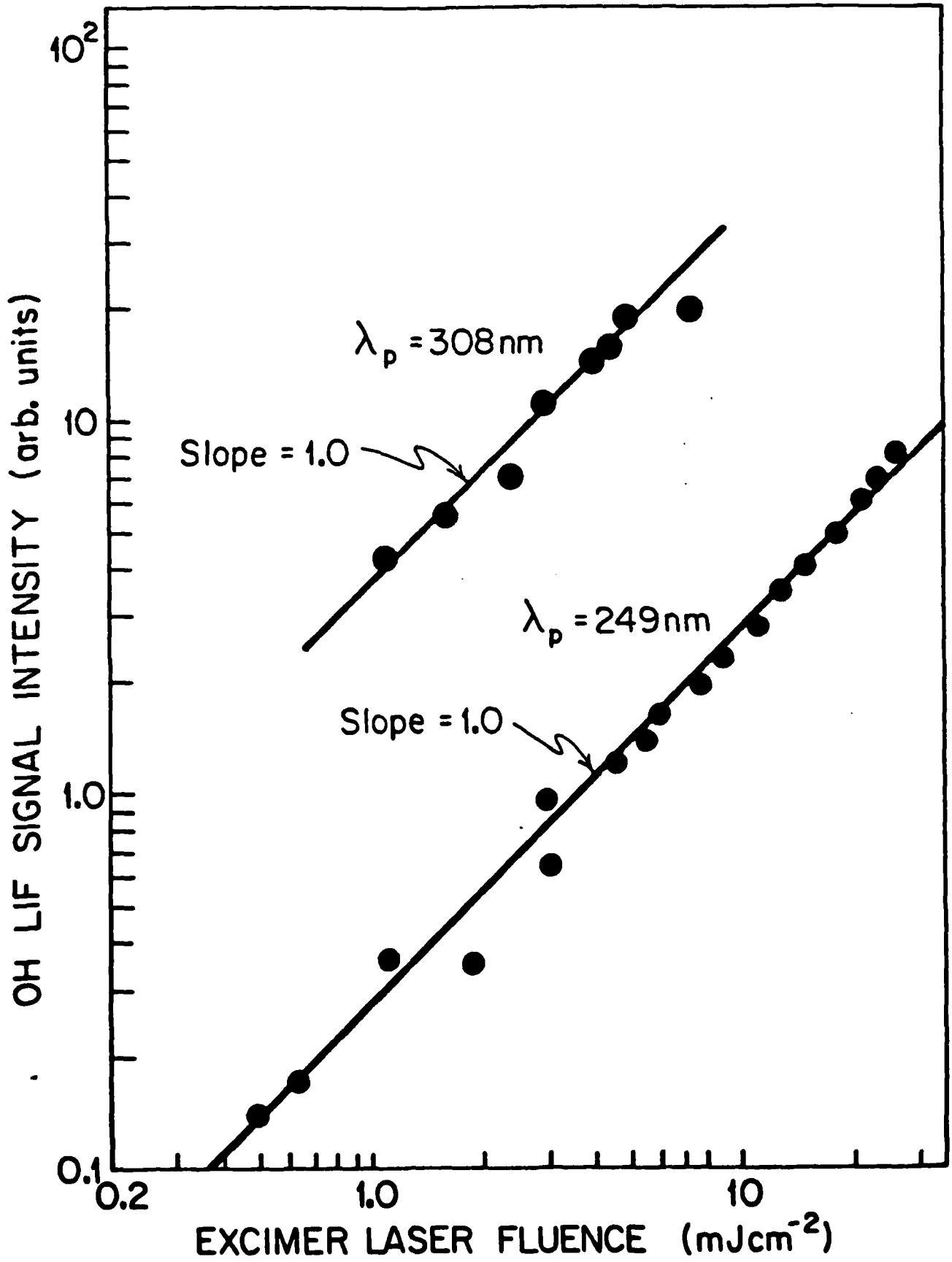
10^2
10
1.0
0.1
0.2
1.0
10
OH LIF SIGNAL INTENSITY (arb. units)
EXCIMER LASER FLUENCE (mJcm^{-2})
λ_p = 308nm
Slope = 1.0
λ_p = 249nm
Slope = 1.0

END

FILMED

3-85

DTIC